Geophys. J. Int. (2001) **145,** 172–186

Ultrasonic *P*- and *S*-wave attenuation in oceanic basalt

M. J. Tompkins* and N. I. Christensen

Department of Geology and Geophysics, University of Wisconsin-Madison, Madison, WI 53706, *USA. E-mail: tompkins@geology.wisc.edu*

Accepted 2000 October 13. Received 2000 October 11; in original form 1999 November 1

SUMMARY

Measurements of compressional wave attenuation are presented for 30 low-porosity ($\phi = 0.4$–8.8 per cent) oceanic basalts collected from 10 oceanic drill holes. The first laboratory measurements of shear wave attenuation in oceanic basalts are presented for 14 rocks from the test suite. For full saturation, attenuation coefficients (α) range from 2.48 to 9.99 dB cm^{-1} for shear propagation and 0.32 dB to 4.69 dB cm^{-1} for compressional propagation at 150 MPa. Q_p and Q_s values range from 14 to 167 and 8 to 27, respectively. Both Q and α show a significant confining pressure dependence to 400 MPa. This pressure dependence is caused by the opening and closing of compliant microcracks. Q and α, both shear and compressional, are also shown to depend on porosity, with α increasing and Q decreasing with porosity. Q_s/Q_p values are reported for 14 samples from the test suite and may be important in determining the degree of saturation when combined with V_p/V_s data. Q_s/Q_p values vary from 0.12 to 0.40 for fully saturated samples. Saturated samples generally display low Q_s/Q_p (<0.4) and high V_p/V_s (>1.75), which is in good agreement with published sandstone Q_s/Q_p data. The mechanisms most likely to be responsible for the observed high *P*- and *S*-wave attenuation are viscous local or 'squirt' flow and to a lesser extent grain boundary frictional sliding. Laboratory data agree well with field seismic measurements of oceanic layer 2A Q_p; however, there is no clear explanation for this agreement, since no single attenuation mechanism has been proven to dominate at both high (MHz) and low (Hz) frequencies. Nevertheless, the good agreement between laboratory and field data suggests that at seismic frequencies the shallow oceanic crust may behave similarly to laboratory samples. One possible explanation is the presence of a different fluid flow mechanism for each frequency scale.

Key words: attenuation, compressional waves, oceans, Q, shear waves.

INTRODUCTION

For most of this century, the field of seismology has strived to understand relationships between seismic observations and the Earth's crustal properties. While correlations between seismic velocities and rock properties have been well established with the implementation of many laboratory studies, ambiguities still exist, because seismic wave velocities are sensitive to many factors such as *in situ* conditions, mineralogy, density and porosity. These ambiguities in velocity lead to quandaries when interpreting seismic data. These problems have been resolved partially by compressional and shear wave velocity ratios (Holbrook *et al.* 1988; Christensen 1996), but more parameters are needed to completely characterize crustal lithologies.

Recently seismologists have studied wave amplitudes in an attempt to illuminate better the relationships between crustal structure and seismic measurements (Jacobson & Lewis 1990; Wilcock *et al.* 1995). The bulk of the related experimental literature has been concerned with quantifying the mechanisms by which seismic energy dissipates in rock, particularly sandstone (e.g. Winkler & Nur 1982; Green *et al.* 1993). In addition to these studies, a few researchers have concentrated on the relationship between wave amplitude and physical properties in crystalline rocks (e.g. Gordon & Davis 1968). Of these studies, fewer still have investigated compressional wave attenuation in oceanic basalt (e.g. Wepfer & Christensen 1990; Tompkins & Christensen 1999). Furthermore, as with velocity studies, shear attenuation measurements in tandem with compressional wave attenuation data (Q_s/Q_p) may be important in interpreting field seismic data.

In contrast to this lack of experimental data, many direct field measurements of seismic wave attenuation in the oceanic crust have been performed in recent years (e.g. Lewis & Jung 1989; Christeson *et al.* 1994; White & Clowes 1994); therefore, experimental studies constraining these field studies are of particular importance. Specifically, laboratory attenuation studies may

*Now at: Geological Engineering Program, Department of Civil and Environmental Engineering, University of Wisconsin-Madison, 1415 Engineering Drive, Madison, WI 53706, USA shed light on *in situ* rock properties (e.g. degree of saturation and porosity). Additionally, laboratory investigations can help determine mechanisms responsible for observed seismic wave energy loss.

The shallow oceanic crust is highly fractured, porous, fluid-saturated rock that is affected by overburden pressures. In order to develop an understanding of any wave amplitude dependence on lithological properties, these *in situ* conditions must be integrated into any experimental study. However, *in situ* environments in the ocean crust vary greatly with depth and proximity to spreading centres. For this reason, it is of paramount importance to evaluate the attenuation properties of water-saturated rock from many locations and depths across the oceans. With the advent of deep sea drilling, it has become possible to sample basalt crustal lithologies from across the world's oceans.

This paper has two objectives.

(1) To characterize the compressional and shear wave attenuation of oceanic basalt better. This work presents measurements of ultrasonic attenuation in 30 oceanic basalts from past Deep Sea Drilling Project (DSDP) cruises.

(2) To use laboratory measurements in determining the effect of rock properties, attenuation mechanisms and fluid saturation on energy loss in low-porosity rock. These experiments, which cover six separate oceanic localities, consist of over 2400 attenuation measurements at confining pressures from 10 to 400 MPa and full water saturation.

PREVIOUS STUDIES

Although laboratory investigations of attenuation in oceanic basalt are sparse, in general many field studies have concentrated on elastic wave absorption in both continental and oceanic basalt. Here we present a brief review of studies conducted on basalts, from which the current study is an extension. These field and laboratory Q studies represent research completed over the past three decades and develop the relationships between rock properties and elastic wave energy loss in basalt that place the current study in proper context. In the current section, quality factor (Q) as well as attenuation (α) will be used to denote energy loss coefficients. In general, Q is inversely proportional to attenuation,

$$\frac{1}{Q} = \frac{\alpha V}{\pi f}, \qquad (1)$$

where $1/Q$ is energy loss per wave cycle, attenuation is energy loss (decibels) per unit length of material, f is frequency and V is velocity. In our convention, attenuation will be used in describing the measurement process, and Q will represent the results.

Field measurements

Direct approaches used to characterize the seismic attenuation in crustal basalts have included spectral analysis of vertical seismic profiles (VSP), waveform spectra inversion from tomographic experiments, refraction and reflection waveform analysis, and sonic log data analysis (Table 1). The frequency range for these experiments was approximately 10–200 Hz, while all but one study considered only a constant-Q (frequency-independent) model.

Several studies have been conducted using vertical seismic profile (VSP) and borehole log data to constrain seismic wave attenuation in the shallow ocean crust (e.g. Rutledge & Winkler 1987; Goldberg & Yin 1994; Goldberg & Sun 1997; Swift *et al.* 1998). Using VSP data from ODP Leg 104, Rutledge & Winkler (1987) determined the Q_p structure of the uppermost basaltic crust (1111 m below sea floor, mbsf) of the Voring Plateau in the eastern Norwegian Sea. Results from their spectral ratio technique include a constant effective Q_p value of ~ 40 and an intrinsic Q_p of >100 for the basalt flows of ODP Site 642 (Table 1). Effective Q is the measured parameter, which includes loss by mechanisms other than rock anelasticity. Rutledge & Winkler (1987) explained that this discrepancy between apparent (effective) and intrinsic attenuation ($1/Q$) is due to scattering and interference effects, caused by strong impedance contrasts. Goldberg & Yin (1994) also demonstrated that while intrinsic attenuation mechanisms (e.g. internal frictional energy loss and viscous fluid flow) may dominate at ultrasonic frequencies, scattering attenuation, due to fracturing and heterogeneity, most probably dominates at low frequencies. Goldberg & Yin (1994) measured an effective Q_p of 8–20 for sonic log and VSP experiments in Hole 735B, while laboratory experiments resulted in a higher Q_p of ~ 20 (Table 1). Recently, Goldberg & Sun (1997) discussed differences in attenuation between intermediate- and slow-spreading oceanic crust by comparing borehole velocity profiles. ODP Holes 504B and 896 A (Pacific Plate) and 395 A (Atlantic Plate) were studied, and results indicate that the degree of vertical heterogeneity strongly affects attenuation (Table 1). Swift *et al.* (1998) presented

Table 1. Reported values for seismic and velocity log Q in oceanic basalt. Note that Q_e is the effective quality factor and Q_i is the intrinsic quality factor (see text).

Reference	Frequency	Location	Reported Q
Rutledge & Winkler (1987)	4–47 Hz	Norwegian Sea (ODP Site 642)	$Q_i > 100$ and $Q_e = 40$
Lewis & Jung (1989)	50–60 Hz	30 km north of Blanco Fracture Zone –Juan de Fuca Ridge intersection	10–16.
Jacobson & Lewis (1990)	1–38 Hz	13 km east of Juan de Fuca Ridge	20–50
Wilcock *et al.* (1992, 1995)	5–80 Hz	East Pacific Rise (9°30′N)	10–20 (off-axis)
Christeson *et al.* (1994)	32–130 Hz	East Pacific Rise (9°30′N)	11–20.
White & Clowes (1994)	11.5 Hz	Endeavor Segment, Juan de Fuca Ridge	20–100
Goldberg & Yin (1994)	15 KHz	Indian Ocean (ODP Hole 735B)	8–20.
Goldberg & Sun (1997)	15 KHz	Pacific (ODP Holes 504B and 896 A) and Atlantic (395 A) oceans	$Q_p = 15$–35 and 5–35 $Q_s = 10$–100
Swift *et al.* (1998)	8–200 Hz	ODP Hole 504B	$Q_i = 8$–10

attenuation data from Hole 504B, and showed that alteration within shallow basalt crust as well as fracturing may produce high values of intrinsic attenuation, although only two thin layers (500–650 mbsf and 800–900 mbsf) within Hole 504B displayed this high attenuation (Table 1).

In addition to down-hole methods, some researchers have relied on refraction data to determine attenuation in the ocean crust (e.g. Lewis & Jung 1989; Jacobson & Lewis 1990; White & Clowes 1994). Lewis & Jung (1989) presented evidence for a frequency-dependent Q_p, which varies between 10 and 50 for the upper crust (Table 1). High crack and void porosity is proposed as a cause for the observed attenuation. The first direct attenuation measurements in the uppermost oceanic crust were performed by Jacobson & Lewis (1990) and focused on young crust off-axis of the Juan de Fuca Ridge. They determined that the upper 650 m of layer 2, composed primarily of pillow basalts, has a very low quality factor (Table 1). In addition to Jacobson & Lewis' (1990) study, White & Clowes (1994) determined the attenuation structure beneath the Endeavor Segment of the Juan de Fuca Ridge. Their attenuation structure has a low Q_p (high attenuation) zone beneath the ridge axis, while Q_p increases to >250 off-axis (Table 1). White & Clowes (1994) showed a correlation between low velocity, high fracture porosity and high attenuation.

Several studies have investigated the shallow attenuation structure of the East Pacific Rise near 9°30′N (i.e. Wilcock *et al.* 1992, 1995; Christeson *et al.* 1994). Although each study addressed slightly different problems, all the results were derived from the same data set. Using a spectral slope method to determine Q_p, Wilcock *et al.* (1995) presented an attenuation structure that consists of an axial low-Q_p anomaly and a higher off-axis Q_p structure. Estimates of Q_p in the uppermost portion of layer 2 are $\sim$10–20, while at depth off the ridge axis, Q_p increases to >500 (Table 1).

Laboratory measurements

As early as 1968, Gordon & Davis attempted to explain the dominant mechanisms for seismic wave energy loss in crystalline rock (including two basalts). From their experiments at high (driven resonance method) and low (cyclic loading stress–strain technique) frequencies, elevated pressures and temperatures, and dry and saturated conditions, they reported several important observations on anelastic energy loss. In dry rock, attenuation proved to be independent of strain amplitude, frequency and mineral composition. Under saturated conditions, attenuation became frequency-dependent and slightly amplitude-dependent for strains above 10^{-6}. Gordon & Davis (1968) also showed that the origin of anelasticity in crystalline rocks lies on grain boundaries.

In agreement with the conclusion of Gordon & Davis (1968), Brennan & Stacey (1977) showed that at low strain amplitudes, basalt shear attenuation is linearly dependent upon strain amplitude; however, they did not discuss specific loss mechanisms.

Tittmann *et al.* (1977) determined the extensional and torsional (shear) quality factor for two lunar analogue basalt samples using a composite resonator technique at elevated pressures. Sample conditions ranged from evacuated (vacuum) to moist (0.4–2 per cent H_2O). Results indicated that low percentages of pore fluid can significantly affect Q (Table 2).

Weiner *et al.* (1987) calculated Q_p in two tholeiitic basalts from the Deccan Traps, India, using the torsional pendulum technique. They contended that viscous sliding at grain boundaries causes relaxation and anelastic energy loss. Measurements at very low frequencies (1.3 Hz) produced Q_s (shear quality factor) values ranging from 25 to >1000, with an attenuation peak at 825 °C due to the transition of silica to a partial melt phase at grain contacts. Similar values of Q_s were determined by Volarovitch & Gurvitch (1957) for two basalts from the USSR.

Finally, using the method described in this study, Wepfer & Christensen (1990, 1991a) presented results from the first laboratory study of oceanic basalt attenuation. They determined the intrinsic attenuation in 10 basalts ranging from vesicular basalts to massive pillows from ocean drilling and ophiolite sampling. Results under saturated conditions and elevated pressures (100 MPa) are presented in Table 2. Q_p values range from 5 for the high-porosity Lau Basin basalt to 295 for sample BO1-208. Wepfer & Christensen (1990, 1991a) related high attenuation (low Q_p) to a high degree of alteration

Table 2. Reported Q-values for laboratory experiments on basalt.

Reference	Technique	Frequency	Sample	Reported Q	Pressure
Volarovitch & Gurvitch 1957	resonant bar	3–4 Hz	two basalts	$Q_s=400, 500$	atmospheric
Gordon & Davis 1968	driven resonance, hysteresis loop	90 KHz	basalt, olivine basalt	$Q_p=170, 250$	unknown
Brennan & Stacey 1977	hysteresis loop	<1Hz	basalt	$Q_s=590$	atmospheric
Tittmann *et al.* 1977	composite resonator	1 kHz	olivine basalt and basalt	$Q_s=1500$ (vacuum), 250 (2 per cent H_2O) and $Q_e=1000$ (vacuum)	75 MPa
Weiner *et al.* 1987	inverted torsion pendulum	1.3 Hz	two tholeiitic basalts	$Q_s=25$ to >1000	atmospheric
Wepfer & Christensen 1990, 1991a	ultrasonic pulse-echo	1 MHz	Juan de Fuca basalt	$Q_p=31$	100 MPa
			five DSDP flow basalts	$Q_p=7$–85	100 MPa
			Lau Basin basalt	$Q_p=8$	100 MPa
			BOI-152 pillow basalt	$Q_p=62$	100 MPa
			BOI-208 basalt	$Q_p=83$	100 MPa
			Oman Ophiolite basalt	$Q_p=124$	100 MPa
Tompkins & Christensen 1999	ultrasonic pulse-echo	1 MHz	Juan de Fuca basalt	$Q_p=11$–17	50 MPa and elevated pore pressures

in combination with high porosities. Additionally, Tompkins & Christensen (1999) showed that elevated pore pressures increase attenuation by as much as 35 per cent in one basalt tested by Wepfer & Christensen (1990).

EXPERIMENTAL METHODOLOGY

In a perfectly elastic non-dispersive medium, wave velocity and amplitude are unaffected by the length or time of travel with the exception of geometric spreading (due to a finite radius source) and scattering. However, earth materials behave as imperfect elastic solids, so wave energy diminishes as a function of time (alternatively, length) by conversion to heat or viscous relaxation. These anelastic mechanisms by which wave energy is lost cause intrinsic attenuation. The term attenuation will be used synonymously with intrinsic attenuation (α); however, the latter term implies that all losses due to scattering and geometric spreading have been removed.

Our approach to measuring both shear and compressional wave attenuation follows that of Wepfer & Christensen (1990) and Winkler & Plona (1982). With this pulse-echo technique, anelasticity is measured by comparing the Fourier amplitude of an ultrasonic pulse, which has travelled through a rock sample, with a reference Fourier amplitude. This is calculated with the equality

$$\alpha(\omega) = 8.68/2L\ln[(R_{23}/R_{12})\{A_1(\omega)/A_2(\omega)\}(1-R_{12}^2)], \quad (2)$$

which represents the spectral ratio method for determining rock attenuation. Here L is the sample length (multiplied by 2 for its two-way travel path), A_1 and A_2 are the reference and sample spectral amplitudes, respectively, R_{23} and R_{12} are reflection coefficients characterizing energy loss at rock–reference interfaces (described below), and the constant 8.68 converts the attenuation coefficient to dB cm^{-1}. Although this equality may be used to determine α directly for both compressional and shear waves, diffraction corrections must be applied to the spectral amplitudes to remove the geometric effects (Winkler & Plona 1982).

The pulse-echo technique described requires that both the rock and reference reflection waveforms be recorded simultaneously. This is accomplished with a piezoelectric transducer that transmits an ultrasonic pulse (compressional or shear mode) through the stacked rock and reference sample assembly shown in Fig. 1. Energy is reflected at each interface and then received by the sending transducer. The resulting reflections from the sample–reference interface and reference–backing piece interface are recorded. Each reflection trace is stacked 32 times to improve the signal-to-noise ratio (snr) before a 3 μs cosine tapered window is applied. Sample reflection waveforms are shown in Figs 2(a) and (b). Finally, the magnitude spectrum for each reflection is calculated (Figs 2c and d) and peak frequency amplitude ratios are used in eq. (2) to calculate attenuation.

The last step in determining attenuation coefficients is to apply diffraction corrections. Each reflection has a distinct correction, which is a function of its wavenumber, transducer radius and travel path (L). The diffraction values used are tabulated in the literature (Benson & Kiyohara 1976 and Khimunin 1972) and applied to both the sample and reference amplitude spectra via a data analysis program developed by Wepfer (1989). The resulting attenuation spectra are shown in Figs 2(e) and (f).

Although many studies have implemented this technique, the proper use of transducer damping rods, reference pieces and backing pieces is not trivial. As shown in Fig. 1, tungsten epoxy damping rods were mounted to the backside of the ultrasonic transducers. These damping rods were used for two purposes: to damp the resonating transducer effectively and to dissipate any energy transmitted from the backside of these transducers completely to avoid unwanted reflections. A brass buffer rod was used as a P-wave reference sample because it has a known high Q (>10 000); however, steel also has a quality factor above

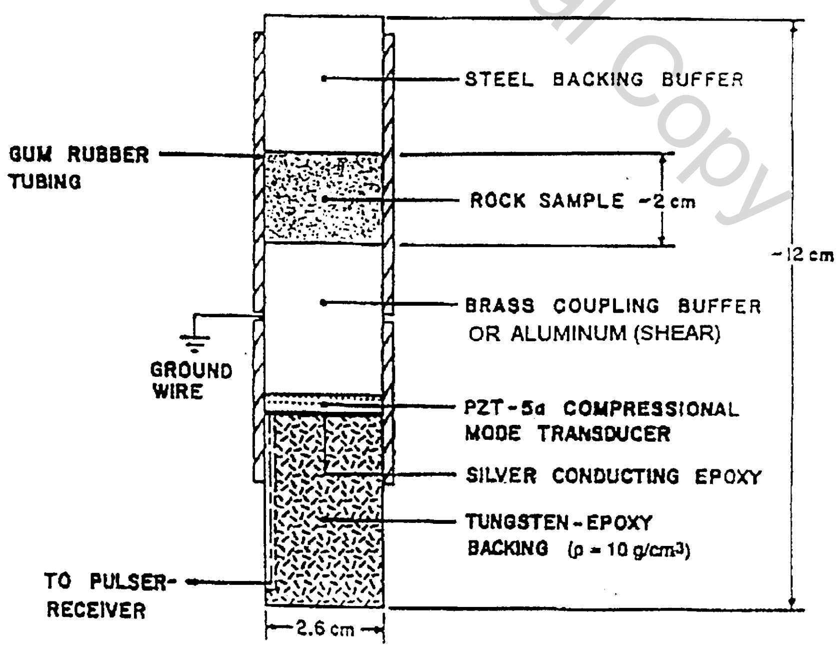

Figure 1. Sample assembly configuration for the pulse-echo method of measuring ultrasonic wave attenuation at elevated pressures. For shear wave attenuation experiments, the brass coupling buffer (reference) is replaced by aluminium.

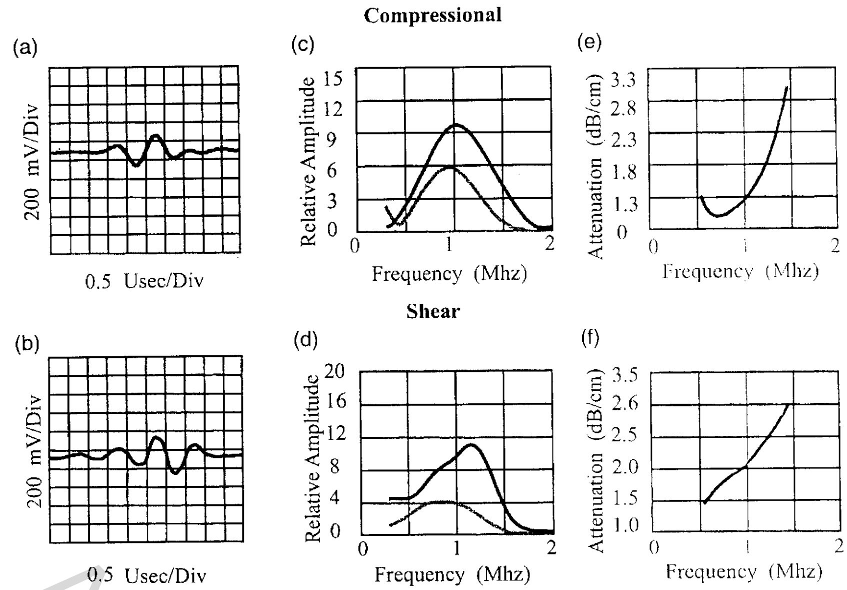

Figure 2. (a,b) Sample compressional and shear waveform records. (c,d) Calculated amplitude spectra for reference (black) and rock (grey) signals in compressional (c) and shear (d) modes. (e,f) Attenuation data results at 1.074 MHz (compressional) and 830 kHz (shear). Relative amplitude and attenuation results are computed using a 3 μs window about the centre of each waveform.

10 000. Brass ($V_p = 4.25$ km s^{-1}, density $= 8.49$ g cm^{-3}) was preferred due to its lower impedance contrast with basalt. This allows for the transmission of more energy to the rock sample, which facilitates more accurate measurements (i.e. a larger snr). Conversely, steel was implemented as a backing piece owing to its high impedance contrast with basalt.

Compressional wave measurements

Compressional wave attenuation was measured in 30 basalt samples. For *P*-wave measurements, the ultrasonic PZT transducers had a centre frequency of 1.074 MHz. All measurements were made at this frequency. Once α is measured, Q_p is derived using eq. (1). In the determination of Q_p, group velocities, measured separately for our samples (Johnston & Christensen 1997), were substituted for phase velocities. This is acceptable since at high frequencies differences between group and phase velocities are slight. The accuracy of calculating α_p using the pulse-echo technique is estimated to be ± 0.05 dB cm^{-1} (Wepfer & Christensen 1990). This sensitivity is determined by comparing the measured attenuation in aluminium with its known small value (<0.0001). This process of calculating Q_p and α_p is repeated at every 10 MPa pressure step between 10 and 400 MPa using the pressure vessel and pumping apparatus described by Christensen (1985).

Shear wave measurements

From our rock suite of 30 basalts, 14 samples had adequate snrs that allowed accurate recording of shear wave reflections (that is, under saturated conditions, shear wave attenuation is higher than compressional wave attenuation). Although the same pulse-echo technique used for compressional wave measurements was employed for shear attenuation measurements, special care had to be taken regarding the sample assembly configuration. In order to obtain the necessary sample reflection used to measure attenuation, as described before, an aluminium buffer rod ($V_s = 3.14$ km s^{-1}, density $= 2.70$ g cm^{-1}) replaced the brass reference used in compressional wave attenuation measurements (See Fig. 1). Using aluminium as the shear wave reference sample proved adequate, since aluminium has a shear impedance very similar to rock. That is, a minimum reflection coefficient is achieved, which allows for maximum energy transmission at the reference–sample interface.

To estimate the error associated with the shear attenuation measurements, the attenuation of brass was calculated. An attenuation value of 0.070 dB cm^{-1} was calculated for brass, presumed to have a true value of zero, which gives an approximate upper limit for error associated with our attenuation measurements. A supplemental result of this accuracy test was the calculation of the shear transducer's centre frequency. The amplitude spectra of aluminium for shear wave propagation displays a peak in amplitude at 830 kHz. In contrast to compressional wave experiments conducted at 1.074 MHz, all shear wave attenuation values were calculated at 830 kHz.

For shear wave data acquisition, compressional wave diffraction corrections were applied to the reference and sample Fourier amplitudes based on their length, wavenumber and radius. Green (1989) showed that the tabulated diffraction corrections (Khimunin 1972; Benson & Kiyohara 1976) for compressional waves generated by a finite piston radiating source can be used for shear wave diffraction corrections with essentially no associated error. This was the assumption for all shear wave attenuation measurements.

Another consideration for shear wave measurements was the effect of pressure on the transducer. The shear transducer, AC-cut quartz, displayed a large decrease in output energy above 150 MPa, so accurate measurements could only be made to this pressure. At pressures above this bound, sample wave amplitudes decreased, generating low snrs. All other aspects of data acquisition and attenuation measurements are identical to those described before for compressional wave measurements.

Sample preparation

Sample preparation involved polishing the rock core (2.5″ diameter cylinder) faces flat to within 0.001″ to ensure good coupling between interfaces in the sample assembly configuration. The rock was then saturated by placing the specimen in distilled water and subjecting it to a vacuum for several days. Experiments were also conducted on several samples that were oven dried. Here samples were placed in a vacuum oven (~80 °C) for 24 hr to ensure complete fluid evacuation. After saturation or drying, the samples were jacketed in copper foil to insulate them from the pressure medium (hydraulic oil). Copper screening was also placed inside the sample jacket (saturated tests only) to allow for fluid to flow from the rock during compression (drained testing). This technique is used to avoid unwanted pore pressure build-up within the rock during pressure fluctuations (see Green 1989).

RESULTS

Sample description

30 basalt samples from 10 DSDP holes were selected for attenuation measurements. Samples were taken from seven drilling sites, including Leg 51, Site 417; Leg 52, Site 417; Leg 53, Site 418; Leg 65, Sites 482, 483 and 485; and Legs 69 and 83, Site 504B. All DSDP sites drilled into oceanic layer 2, encountering basalt of various ages (<3 Ma to 110 Ma), and, consequently, proximities to oceanic spreading ridges. The samples were chosen because they span a wide range of ages as well as physical properties. Two main criteria were used in selecting the test suite from a sample body of some 160 cores. First, samples were chosen that accurately characterize the range of physical properties at each site; that is, the sample set represents the widest range of physical properties. Second, because a limited number of cores could be tested, samples were selected from depth intervals that allowed for maximum coverage at each site. These samples are representative of a large variation in oceanic basalts and constrain the ultrasonic properties of oceanic layer 2. Johnston & Christensen (1997) completed a detailed physical properties study of these DSDP basalts including measurements of compressional and shear wave velocities. This data set, abbreviated in Table 3, was used for the calculation of both compressional and shear wave Q from eq. (1).

Velocities

In order to calculate the ultrasonic wave quality factor (Q) represented by eq. (1), velocity must be known as a function of pressure, since any pressure dependence is of fundamental importance in measuring rock attenuation (Toksoz *et al.* 1979). An abbreviated tabulation of basalt compressional and shear

Table 3. Physical property data for DSDP samples.

Sample	Location	Depth (mbsf)	Age (Ma)	Density (kg m^{-3})	Porosity (%)	V_p at 200 MPa (km s^{-1})	V_s at 200 MPa (km s^{-1})
417A-25–1	Bermuda Rise	227	110	2565	8.8	4.775	2.558
417A-30–4	Bermuda Rise	275	110	2803	2.8	5.589	3.03
417A-37–1	Bermuda Rise	341	110	2824	2	6.054	3.285
417A-42–6	Bermuda Rise	388	110	2710	4.3	5.316	2.877
417D-28–5	Bermuda Rise	386	110	2706	0.6	6.132	3.22
417D-37–2	Bermuda Rise	454	110	2809	2.8	5.777	3.134
417D-58–3	Bermuda Rise	620	110	2671	5.8	4.882	2.513
418A-35–1	Bermuda Rise	458	110	2679	3.8	5.054	2.775
418A-46–1	Bermuda Rise	544	110	2800	1	5.925	3.284
418A-55–2	Bermuda Rise	622	110	2923	2.7	6.036	3.358
418A-71–1	Bermuda Rise	753	110	2930	2	6.145	3.453
418A-85–2	Bermuda Rise	852	110	2956	0.4	6.416	3.508
482B-16–2	Gulf of California	168	<3	2958	1.3	6.384	3.539
482C-10–3	Gulf of California	143	<3	2920	2	6.048	3.352
482C-13–2	Gulf of California	163	<3	2955	1.2	6.309	3.49
482D-9–1	Gulf of California	141	<3	2961	0.8	6.294	3.518
483–20–1	Gulf of California	169	<3	2956	1.6	6.329	3.511
483–26–2	Gulf of California	203	<3	2910	1.9	5.893	3.316
483B-4–4	Gulf of California	126	<3	2967	1.7	6.209	3.42
483B-19–3	Gulf of California	208	<3	2911	2.6	5.911	3.28
483B-25–2	Gulf of California	233	<3	2868	3.6	5.512	3.09
485A-12–1	Gulf of California	155	<3	2985	1.7	6.360	3.514
485A-23–4	Gulf of California	217	<3	2939	2.7	5.873	3.204
485A-35–1	Gulf of California	286	<3	2954	1.5	6.160	3.419
504B-15–4	Costa Rica Rift	381	6	2877	2.5	6.012	3.312
504B-22–1	Costa Rica Rift	431	6	2830	2.7	6.041	3.305
504B-28–3	Costa Rica Rift	479	6	2853	4.2	5.794	3.194
504B-75–1	Costa Rica Rift	872	6	2862	1.9	5.887	3.261
504B-84–2	Costa Rica Rift	948	6	2943	1.2	6.509	3.583
504B-91–2	Costa Rica Rift	1005	6	2960	0.8	6.432	3.532

wave velocities appears in Table 3 and shows the wide range of values associated with our test samples. Both shear and compressional velocities increase with increasing density and decrease as a function of increasing porosity. This result is consistent with published data for many rock types (e.g. Birch 1960; Christensen 1972).

Fig. 3 shows velocity versus pressure curves for four basalts from the test suite. Complete velocity data for every sample are given by Johnston & Christensen (1997). In Fig. 3(a), compressional wave velocities are shown for samples 504B84R2 and 483B4R4, while shear wave data are plotted for samples 418A46R1 and 482B16R2 in Fig. 3(b). Both V_p and V_s curves show the typical exponential relationship with pressure, which is due to the closure of microcracks (e.g. Birch 1960; Kowallis *et al.* 1982). This observed microcrack closure dependence of velocity is important, because it illuminates the necessity to measure dynamic wave properties at multiple pressures; that is, if properties are determined at only atmospheric pressures, *in situ* properties will be inaccurately estimated.

Saturated experiments

Saturated attenuation, density and porosity data for the 30 samples included in the test suite are summarized in Table 4 at six pressures. At 50 MPa, P-wave attenuation values range

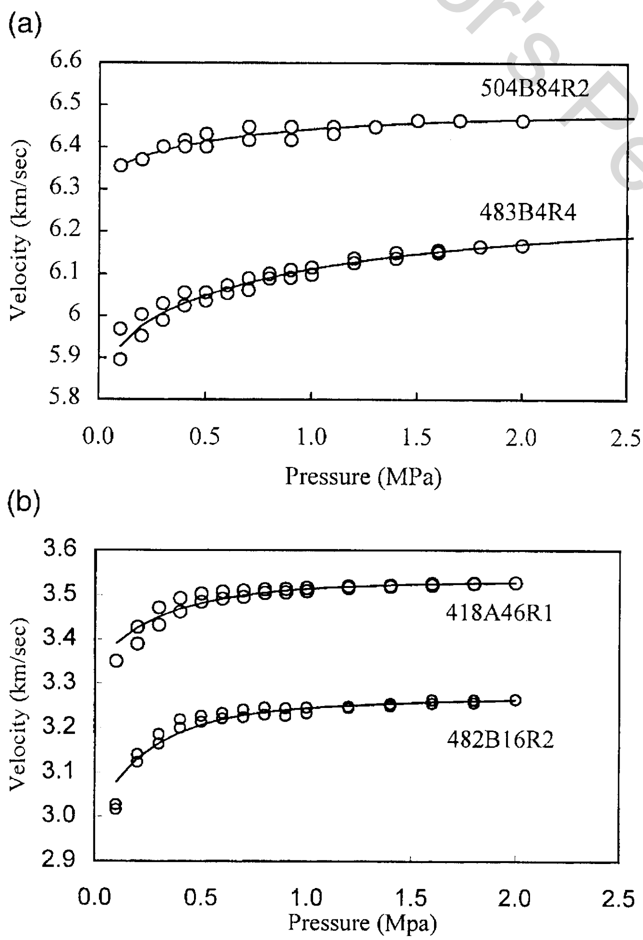

Figure 3. (a) Basalt compressional wave velocity versus pressure for two samples. (b) Basalt shear wave velocity versus pressure data. Solid lines are non-linear weighted least-squares fits to raw data using the method of Wepfer & Christensen 1991b).

from 0.41 dB cm^{-1} for sample 504B84R-2 to 4.96 dB cm^{-1} for sample 417A25R-1. Q_p calculations at 50 MPa presented in Table 5 accentuate the differences between basalt samples with values ranging from 12 to 112. At 300 MPa, P-wave attenuation values show a range from 0.22 dB cm^{-1} ($Q_p=210$) to 3.88 dB cm^{-1} ($Q_p=16$). The range of Q-values actually increases with pressure, which is due to the differing pressure dependences between sample velocities.

Fig. 4 shows compressional wave attenuation data versus pressure for eight basalt samples and emphasizes the extension of pressure dependence to wave energy loss. Fig. 4 presents data for samples that exhibit the maximum and minimum measured P-wave attenuation as well as samples from each DSDP site. Several trends in compressional wave attenuation data are apparent from inspection of Fig. 4. First, attenuation shows a sharp decrease with increasing pressure. As mentioned previously, velocity results increase exponentially with increasing pressure, while attenuation decreases with pressure. Also, the data plotted in Fig. 4 do not share the same pressure relationship. While samples 417D58R-3 and 417A42R-6 decrease sharply with pressure, samples 504B91R-1, 48326R-2 and others show a much shallower decrease with pressure. The range of attenuation values decreases as a function of increasing pressure in Fig. 4, which implies that high-aspect-ratio microcrack porosity is at least partially responsible for observed rock anelasticity. Coupling between transducers, references and samples may also improve with increasing pressure and act to decrease the range of attenuation. However, these coupling effects are minimized above small confining pressures (approximately 10 MPa). This is substantiated by the negligible change in amplitude of the brass and aluminium reference signals above this pressure.

Shear attenuation measurements were limited to 14 samples from our test suite. As a result, a bias was imposed when selecting samples for shear attenuation measurements, because only samples which had high Q_s values could be chosen. Therefore, shear attenuation sample porosities and densities show less variation than for compressional waves (Table 4). Results are presented for these samples in Table 4. Under saturated conditions, intrinsic energy loss for shear waves is much higher than for compressional waves, and like compressional wave attenuation results, the range of attenuation values for shear waves is large (2.49–10.46 dB cm^{-1} at 100 MPa).

To demonstrate the dependence of shear wave attenuation on pressure, Fig. 5 shows attenuation–pressure data for five basalt samples. As with compressional wave attenuation, shear wave results display a wide range of pressure dependences. Although sample 417D28R5 decreases non-linearly with pressure, the other samples in Fig. 5 are more representative of shear attenuation results. All but four samples show a linear decrease in attenuation with pressure. This result is not unexpected given the relatively low pressures at which attenuation was measured (150 MPa). At these low pressures, microcrack closure is probably not complete; consequently, attenuation has not asymptotically approached a minimum value. The P-wave attenuation data in Fig. 4 show a similar relationship below 100 MPa confining pressure.

Dry experiments

Although rock property experiments on oceanic rocks are undoubtedly more appropriate under saturated conditions, P-wave attenuation measurements were conducted on two

Table 4. Shear and compressional wave attenuation, porosity and density data at several pressures. Samples are water-saturated unless otherwise noted.

Sample	Density (kg m^{-3})	Porosity (%)	50 MPa		100 MPa		150 MPa		200 MPa Alpha-P	300 MPa Alpha-P	400 MPa Alpha-P
			Alpha-P	Alpha-S	Alpha-P	Alpha-S	Alpha-P	Alpha-S			
417A-25–1	2565	8.8	4.96		4.76		4.40		4.24	3.88	
417A-25–1 Dry	2476	8.8	4.24	6.84	3.93	5.74	3.96	4.71	3.83	3.60	
417A-30–4	2803	2.8	2.25		2.04		1.91		1.83	1.90	1.87
417A-37–1	2824	2.0	1.97		1.69		1.53		1.42	1.31	
417A-42–6	2710	4.3	4.38		3.80		3.47		3.22	2.87	2.64
417D-28–5	2706	0.6	1.13	12.92	0.95	10.46	0.89	8.37	0.81	0.79	0.74
417D-37–2	2809	2.8	2.17		2.00		1.86		1.78	1.62	1.57
417D-58–3	2671	5.8	4.70		3.80		3.34		3.13	2.72	
418A-35–1	2679	3.8	3.06		2.66		2.40		2.24	1.95	
418A-46–1	2800	1.0	0.83	9.09	0.78	7.49	0.80	5.54	0.76	0.69	0.67
418A-55–2	2923	2.7	1.01		0.93		0.93		0.85	0.73	0.77
418A-71–1	2930	2.0	1.53		1.30		1.17		1.04	0.87	0.80
418A-85–2	2956	0.4	2.18		1.81		1.60		1.53	1.42	
482B-16–2	2958	1.3	0.73	3.79	0.63	3.10	0.58		0.54	0.49	0.46
482C-10–3	2920	2.0	1.88		1.79		1.71		1.63	1.58	
482C-13–2	2955	1.2	0.85	5.31	0.75	4.09	0.69		0.68	0.64	0.65
482D-9–1	2961	0.8	0.53	4.53	0.43	3.66	0.35		0.30	0.34	0.36
483–20–1	2956	1.6	0.85	5.99	0.77	5.17	0.71	4.27	0.69	0.66	0.60
483–26–2	2910	1.9	1.04	9.55	0.97	7.88	0.89		0.88	0.72	0.68
483B-4–4	2967	1.7	0.68		0.54		0.45		0.41	0.35	0.32
483B-19–3	2911	2.6	3.08		2.91		2.70		2.51	2.27	1.98
483B-25–2	2868	3.6	1.47	4.74	1.23	4.65	1.00	4.83	0.82	0.58	0.45
485A-12–1	2985	1.7	0.51	5.21	0.44	4.95	0.47	4.47	0.42	0.40	0.32
485A-12–1 Dry	2968	1.7	0.86	2.87	0.77	2.49	0.54		0.51	0.36	
485A-23–4	2939	2.7	2.18		1.94		1.87		1.78	1.70	1.63
485A-35–1	2954	1.5	1.64	5.53	1.46	4.51	1.29	3.43	1.12	0.95	
485A-35–1 Dry	2921	1.5		1.48		1.32		0.78			
504B-15–4	2877	2.5	1.92		1.64		1.40		1.41	1.33	1.23
504B-22–1	2830	2.7	3.29		3.05		2.95		2.92	2.74	2.57
504B-28–3	2853	4.2	2.66		2.27		2.00		1.79	1.55	1.46
504B-75–1	2862	1.9	1.17		0.99		0.90		0.88	0.69	
504B-84–2	2943	1.2	0.41	3.35	0.41	2.80	0.40	1.74	0.39	0.41	
504B-91–2	2960	0.8	0.45	5.40	0.35	4.21	0.27		0.22	0.22	

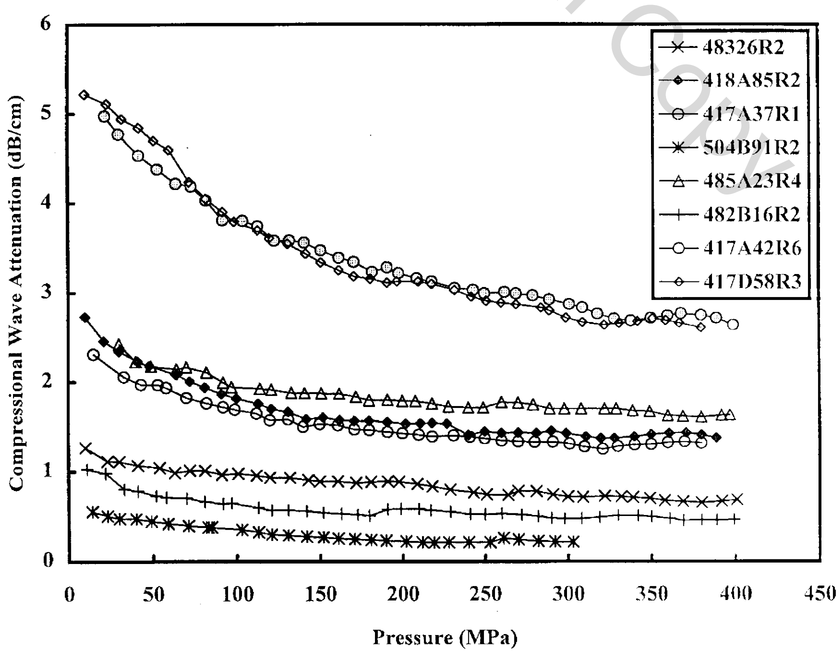

Figure 4. Compressional wave attenuation results plotted versus pressure for eight basalt samples.

Table 5. Basalt Q_p, Q_s and Q_s/Q_p data at several pressures. Samples are water-saturated unless otherwise noted.

Sample	50 MPa			100 MPa			150 MPa			200 MPa	300 MPa	400 MPa
	Q_p	Q_s	Q_s/Q_p	Q_p	Q_s	Q_s/Q_p	Q_p	Q_s	Q_s/Q_p	Q_p	Q_p	Q_p
417A-25-1	12.8			13.2			14.2			14.6	15.9	
417A-25-1 Dry	15.2	12.2	0.8	16.2	14.3	0.9	16.0	17.3	1.1	16.4	17.4	
417A-30-4	23.8			26.1			27.7			28.9	27.6	28.0
417A-37-1	25.2			29.0			32.0			34.3	37.3	
417A-42-6	13.1			14.8			16.1			17.3	19.3	20.9
417D-28-5	43.2	5.2	0.1	50.9	6.4	0.1	54.5			59.3	61.2	65.5
417D-37-2	24.0			25.7			27.7			28.9	31.7	32.6
417D-58-3	13.6			16.4			18.4			19.5	22.2	
418A-35-1	19.8			22.4			24.5			26.1	29.8	
418A-46-1	60.5	7.3	0.1	64.0	8.8	0.1	62.7	11.8	0.2	65.8	72.7	74.1
418A-55-2	49.2			52.7			53.0			57.9	66.4	63.3
418A-71-1	31.9			37.4			41.1			46.0	55.2	59.9
418A-85-2	21.7			25.8			28.9			30.0	32.2	
482B-16-2	64.1	16.3	0.3	71.7	19.6	0.3	85.8			79.3	97.4	99.6
482C-10-3	26.5			27.5			28.6			30.1	31.0	
482C-13-2	55.8	11.7	0.2	62.9	15.1	0.2	68.3			69.3	73.1	72.0
482D-9-1	89.4	13.6	0.2	108.9	16.7	0.2	133.3					
483-20-1	55.3	10.2	0.2	61.1	11.8	0.2	65.6	14.3	0.2	67.6	70.3	77.3
483-26-2	48.7	6.8	0.1	51.7	8.3	0.2	56.5			56.7	69.5	72.9
483B-4-4	71.0			89.4			105.4			116.8	137.1	
483B-19-3	16.4			17.2			18.5			19.9	21.9	25.0
483B-25-2	37.5	15.1	0.4	44.1	15.2	0.3	53.9	14.7	0.3	65.4	91.9	117.1
485A-12-1 Sat	93.2	11.9	0.1	107.1	12.4	0.1	99.9	13.7	0.1	109.5	115.6	143.9
485A-12-1 Dry	56.4	21.2	0.4	62.7	24.4	0.4	88.8	27.8	0.3	93.9	133.1	
485A-23-4	23.7			26.2			27.0			28.1	29.4	30.4
485A-35-1 Sat	29.6	11.4	0.4	32.9	13.9	0.4	37.2	18.2	0.5	42.6	50.3	
485A-35-1 Dry		43.1			48.0							
504B-15-4	26.3			30.4			35.4			35.0	37.1	40.1
504B-22-1	14.9			16.0			16.5			16.6	17.6	18.8
504B-28-3	19.6			22.6			25.5			28.4	32.4	34.2
504B-75-1	42.8			50.1			54.9			56.5	72.1	
504B-84-2	111.5	18.5	0.2	111.0	22.0	0.2	114.2	35.2	0.3	117.9	110.0	
504B-91-2	103.2	11.7	0.1	129.8	14.8	0.1	168.9			205.3	210.1	

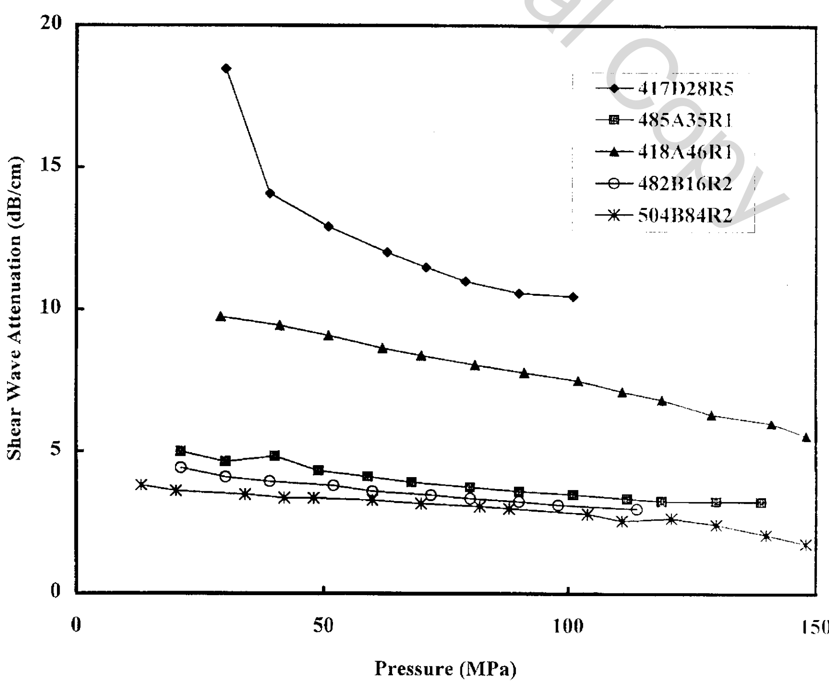

Figure 5. Shear wave attenuation results for five basalt samples.

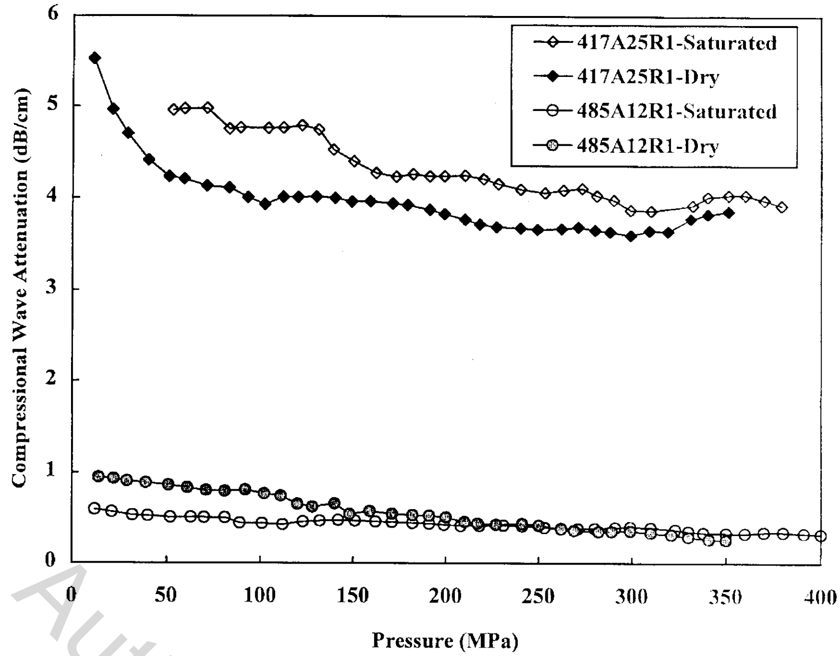

Figure 6. Compressional wave attenuation versus pressure for two samples under dry and saturated conditions.

samples under oven-dry conditions to aid in the interpretation of attenuation mechanisms dominating in dry rock and to constrain Q_s/Q_p dependence on saturation. Attenuation results for both saturated and dry experiments are shown in Table 4 and Fig. 6 for samples 417A25R1 and 485A12R1. As predicted by Winkler & Nur (1982), sample 485A12R1 has a lower attenuation coefficient under saturated conditions and low pressures, but this sample shows a higher attenuation coefficient for the saturated run at higher pressures. Sample 417A25R1 shows higher attenuation under saturated conditions regardless of pressure. Results for sample 417A25R1 and sample 485A12R1 (above 250 MPa) are in agreement with dry and saturated attenuation data presented by Wepfer & Christensen (1991a) for several low-porosity basalts.

In addition to dry *P*-wave attenuation measurements, *S*-wave experiments were completed for three dry samples: samples 417A25R1, 485A12R1 and 485A35R1. Dry shear attenuation results are presented in Table 4 and Fig. 7 as a function of pressure. Because shear attenuation is maximized under saturated conditions, measurements on sample 417A25R1 (dry $Q_s = 17$ at 150 MPa) could not be performed under a saturated state (the sample reflection could not be differentiated from noise),

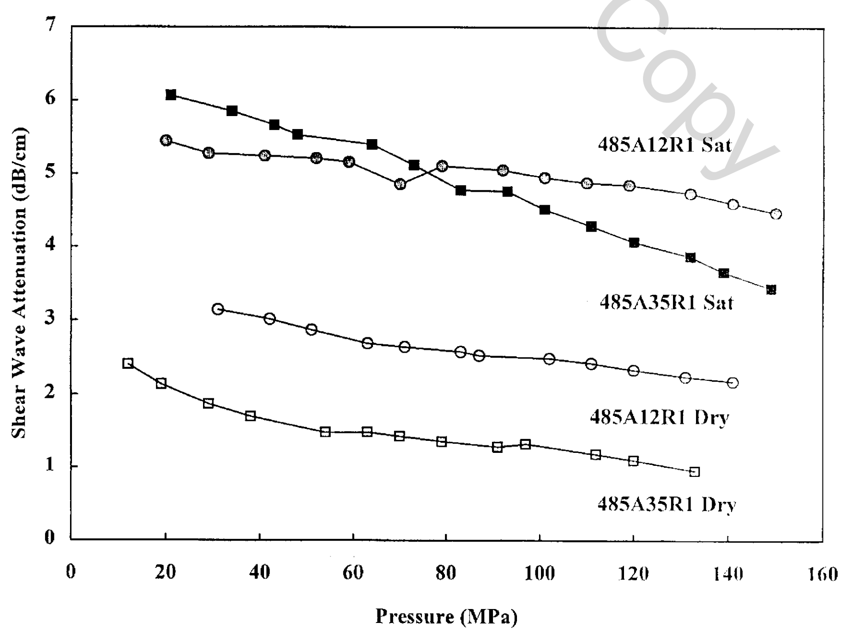

Figure 7. Dry and saturated shear wave attenuation data plotted versus pressure to 200 MPa.

and it is left out of Fig. 7. Fig. 7 shows the effect of saturation on shear attenuation, while it is obvious that shear wave attenuation is minimized under dry conditions.

Because Q calculations scale attenuation measurements by sample velocities, variations between basalt properties can be illuminated by inspecting Q data. Fig. 8 presents Q_p results versus pressure for the same eight samples plotted in Fig. 4. Q_p versus pressure data exhibit similar relationships to attenuation results; however, Q_p data trends are inverted from those of attenuation: Q_p values increase with pressure and the range between sample values increases at high pressures. Q_p versus pressure relationships shown in Fig. 8 have been documented by laboratory attenuation studies of basalt as well as other rock types (e.g. Wepfer & Christensen 1991a; Johnston & Toksoz 1980).

Shear wave Q is plotted in Fig. 9. Again, basalt anelastic behaviour is accentuated due to the relationship between Q and velocity. For example, while sample 504B84R2 has a relatively small attenuation coefficient (see Fig. 5), which varies little with pressure, Q_s results show a large pressure dependence. As with the Q_p results, the range of Q_s values between samples also increases with pressure (Fig. 9).

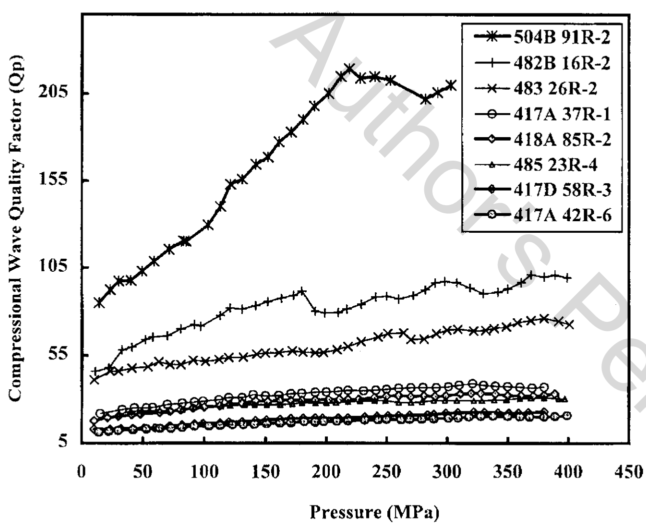

Figure 8. Basalt compressional wave quality factor (Q_p) versus pressure to 400 MPa. Q_p curves are listed in decreasing order.

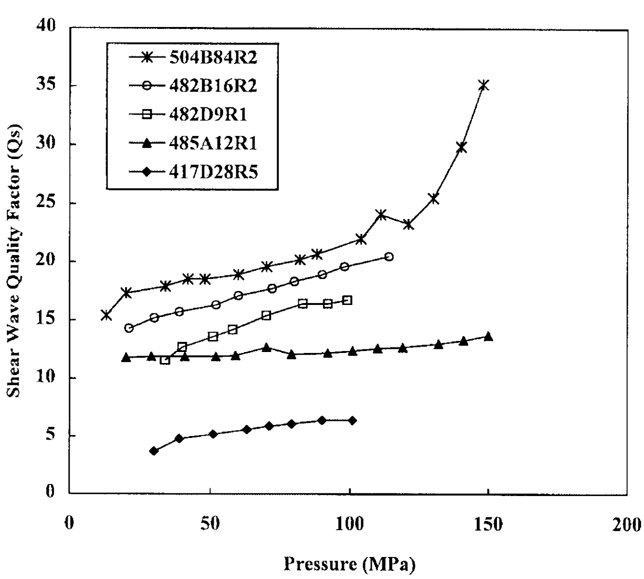

Figure 9. Basalt shear wave quality factor (Q_s) plotted versus pressure to 200 MPa for five samples.

DISCUSSION

Attenuation mechanisms

Biot (1956) presented numerical solutions for wave propagation in porous solids containing a viscous fluid phase. Biot demonstrated that above a critical frequency, propagating stress waves cause relative motion between the rock frame and pore fluid, which results in energy loss. Mavko & Nur (1979) developed a second model for viscous 'squirt' flow in partially saturated porous rock. In their model, pore fluid within partially gas-filled compliant cracks (high aspect ratio) is forced out into stiff pore spaces (low aspect ratio) when a stress wave compresses the compliant crack. Again this mechanism has a diagnostic frequency dependence. More recently, Dvorkin & Nur (1993) developed a unified theory describing a combined Biot and 'squirt' flow attenuation mechanism. In their work, Dvorkin & Nur (1993) determined that sandstone anelasticity can be more accurately characterized by accounting for both micromechanical mechanisms. Walsh (1966) developed the theory for rock internal frictional energy loss and hypothesized that stresses induced by the propagation of elastic waves cause the relative motion of juxtaposed grains (thin cracks). This relative motion produces heat that relaxes the rock frame and dissipates energy. Grain boundary friction is a frequency-independent attenuation mechanism.

While no quantitative discussion of attenuation mechanisms affecting our basalt samples will be made, differences between dry and saturated attenuation data lend themselves to the qualitative discussion of mechanisms dominating for each condition. Data for dry and saturated P- and S-wave attenuation experiments (Table 4) for samples 417A25R1 and 485A35R1 show an increase in attenuation for water-saturated samples. Sample 485A12R1 has higher attenuation values for dry conditions at low pressures (<250 MPa), but values for the dry state are greater than those under saturated conditions at higher pressures. Less loss for P and S waves in dry rock implies that under saturated conditions fluid flow is responsible for a large portion of the observed anelasticity. For example, sample 485A35R1 shows a 30 per cent increase in S-wave attenuation under saturated conditions. P-wave attenuation in 485A12R1 increases by 62 per cent when it is saturated. Because this phenomenon of higher attenuation persists to elevated pressures, a 'squirt' flow mechanism is probably not exclusively responsible for the observed energy loss. A Biot-type fluid flow mechanism is also likely to contribute to attenuation in our samples.

Another observation that can help constrain what mechanisms control basalt attenuation is the dependence of a sample's attenuation on pressure. Gordon & Davis (1968) showed that attenuation in dry crystalline rocks decreases to nearly zero at elevated differential pressures (200 MPa). They interpreted this result to imply that frictional sliding, which was the only attenuation mechanism considered, was prohibited at high pressure, so attenuation decreased to zero. As shown in Table 4, this is not the case for our basalts. The result that attenuation is

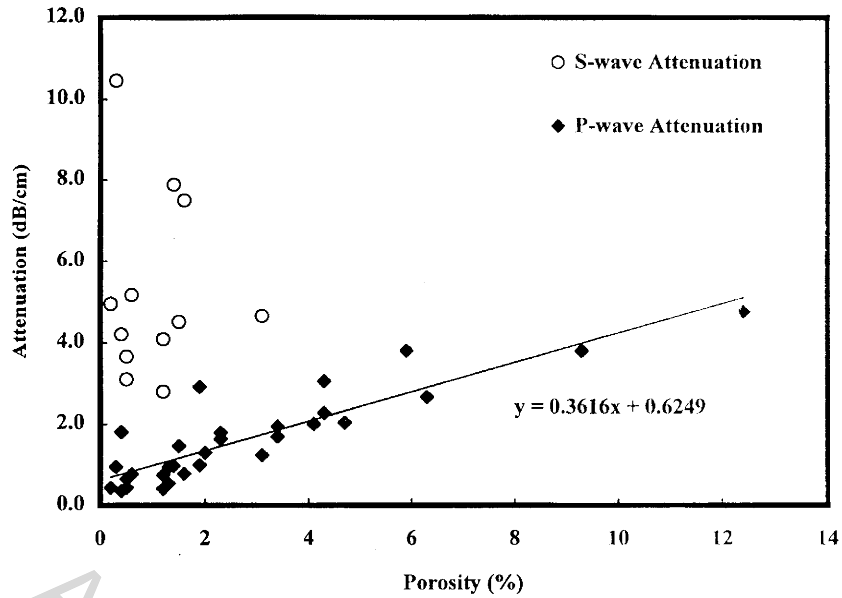

Figure 10. Compressional and shear wave attenuation as a function of porosity at 100 MPa. The linear regression was determined only for compressional wave data. Porosity has an estimated error of ± 0.4 per cent (see Hyndman *et al.* 1979).

non-zero in both saturated and dry rock at elevated pressure implies that a mechanism other than frictional dissipation dominates low-porosity oceanic basalts (Walsh 1966).

Porosity and density effects

As observed by Wepfer & Christensen (1991a), basalt ultrasonic wave attenuation is dependent on rock physical properties such as porosity and density. Lewis & Jung (1989) speculated that this phenomenon may exist at seismic frequencies also. To address the extension of this observation to our test suite, results of saturated basalt attenuation at 100 MPa are plotted against porosity in Fig. 10. As expected from the pressure dependence of attenuation, α increases with increasing porosity. Although the data in Fig. 10 show some scatter, a linear trend with porosity is recognizable in the *P*-wave attenuation data. *P*-wave attenuation data are plotted against density in Fig. 11. Here the correlation between attenuation and density is not as clear; however, attenuation does show a tendency to decrease with increasing density. The relationships between *S*-wave attenuation, porosity and density are also shown in Figs 10 and 11. In contrast to *P*-wave attenuation results, *S*-wave attenuation shows a less clear trend with porosity and density at 100 MPa pressure. This is due to the bias in selecting samples for *S*-wave measurements (that is, only low-porosity samples were tested). Both an increase in attenuation with porosity and a decrease with density are a result of pore fluid effects on attenuation. Many attenuation mechanisms active in saturated rock originate from the viscous behaviour of the pore fluid. For this reason, less pore fluid generally results in less energy loss.

Q_s/Q_p

Data from many laboratory studies of attenuation in sedimentary rock show that under partially saturated conditions Q_s/Q_p is greater than 1. For completely saturated rock, Q_s/Q_p is less than 1 (Winkler & Nur 1982; Murphy 1982). The model for

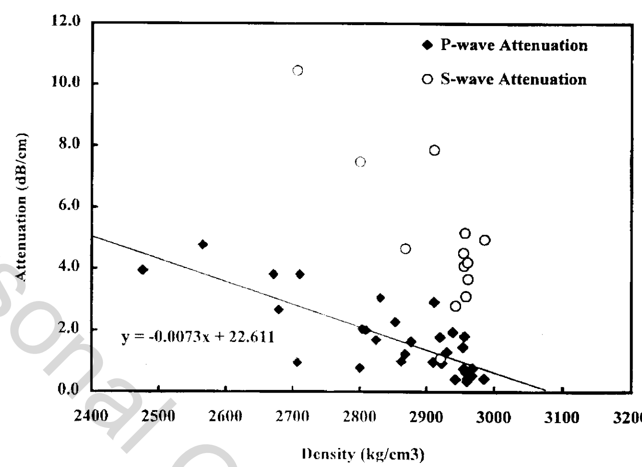

Figure 11. Compressional and shear wave attenuation data as a function of density at 100 MPa. The linear fit was calculated for compressional wave data only.

this inversion of Q_s/Q_p ratios involves the 'squirt' flow mechanism. Under saturated conditions, pure shear compresses some cracks and not others, inducing more crack-to-crack fluid flow than does a compressional wave, which compresses all cracks equally. This increase in local flow increases shear attenuation in relation to compressional attenuation. Under partial saturation, pure shear induces viscous flow within some cracks and not others; however, compressional waves induce flow within all cracks, because a compressible fluid phase (air) is present when the crack is compressed and allows fluid to flow within the crack. In dry rocks, shear attenuation is equal to or larger than compressional wave attenuation. Data presented in this study for a high-porosity basalt (417A25R1) support these conclusions.

Both dry and saturated Q_s/Q_p were measured for sample 485A12R1; however, saturated Q_s/Q_p values for 12 other samples (Table 5) were determined. Additionally, the dry Q_s/Q_p for sample 417A25R1 was calculated (Table 5). Values for saturated Q_s/Q_p ranged from 0.12 to 0.46 at 150 MPa for samples 485A12R1 and 485A35R1, respectively. For dry conditions, Q_s/Q_p is 1.10 and 0.30 for samples 417A25R1 and 485A12R1. From these data, it is apparent that high-porosity basalt (417A25R1; $\phi=8.8$ per cent) shows a shear quality factor identical to the compressional wave quality factor, which has been observed by Gardner *et al.* (1964). However, in a low-porosity sample (485A12R1; $\phi=1.7$ per cent) shear wave Q is still lower than compressional wave Q. Under saturated conditions, Q_s is less than Q_p for all samples tested. This result suggests that for low-porosity dry basalt, a mechanism other than fluid flow increases shear wave loss. As mentioned before, this mechanism could be frictional sliding.

In addition to illuminating the importance of different attenuation mechanisms, Q_s/Q_p may be used to characterize a rock's saturation state. To accomplish this, Winkler & Nur (1982) plotted data for Q_s/Q_p versus V_p/V_s. Their results for sandstones indicate that a small Q_s/Q_p (<1) in combination with a small V_p/V_s (<1.75) is characteristic of dry sample conditions. In addition, a slightly smaller Q_s/Q_p and a higher V_p/V_s (>2) indicates a fully saturated sample. In Fig. 12, Q_s/Q_p and V_p/V_s data from Winkler & Nur (1982), Toksoz *et al.* (1979) and the current study are compared. It is evident from Fig. 12 that samples that are dry have higher Q_s/Q_p (>0.40) and lower V_p/V_s (<1.75). Although no data are presented for partially saturated conditions, it is clear that the combination of Q_s/Q_p and V_p/V_s can more accurately characterize the saturation state of rock than either ratio alone.

Scaling to seismic frequencies

As demonstrated before, ultrasonic attenuation ($1/Q$) is strongly dependent on microcrack porosity. However, field measurements (seismic frequencies) are most likely to be affected by large-scale fracturing and heterogeneities (Goldberg & Yin 1994; Goldberg & Sun 1997). Another mechanism responsible for seismic wave energy loss is scattering (Rutledge & Winkler 1987; Goldberg & Yin 1994). Wepfer (1989) showed that scattering does not occur at ultrasonic frequencies because the ratio of wavelength to grain size (2.1–104) is large. In addition, Winkler & Nur (1982) suggested that for low strain amplitudes ($<10^{-6}$) frictional sliding is not a dominant mechanism for energy loss. Seismic frequencies produce strains well below this threshold, so this mechanism responsible for ultrasonic wave attenuation most probably does not scale up to seismic frequencies. Swift *et al.* (1998) did give support for the occurrence of intrinsic attenuation at VSP frequencies, but specific mechanisms for such attenuation were not discussed. More recently, Shapiro & Muller (1999) theorized that an effective seismic permeability attenuation mechanism could produce significant energy loss at seismic frequencies below critical scattering frequencies. In contrast to Biot's 'global flow' mechanism, this mechanism describes 'local flow' about heterogeneities. However, Shapiro & Muller's (1999) model is highly dependent upon scale of heterogeneity and frequency also.

Although it is uncertain whether energy loss is dominated by similar mechanisms between ultrasonic and seismic scales (Winkler & Nur 1982), data from both frequency ranges show remarkably good agreement for our basalts. Comparison of Table 1 and the current data set (Table 5) shows that the bulk of Q_p values at the ultrasonic scale (14–166 at 150 MPa) fall within the range of seismic Q_p measurements for layer 2A (10–100). This, taken with the fact that our laboratory-scale velocity–density relationships follow a similar trend to borehole-scale velocity–density relationships (see Carlson & Herrick 1990), suggests that basalt formations may have similar structures to laboratory samples. That is, rock properties, including attenuation, may scale upwards with wavelength. In this case, a fluid flow mechanism is the most probable intrinsic mechanism common between seismic and ultrasonic scales.

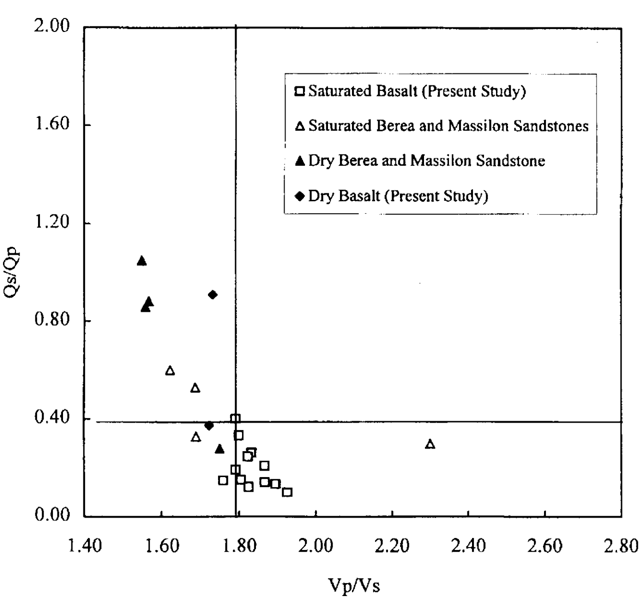

Figure 12. Q_s/Q_p and V_p/V_s data presented for oceanic basalts (present study), Berea Sandstone (Toksoz *et al.* 1979) and Massilon Sandstone (Winkler & Nur 1982). Dry conditions are represented by open symbols, while closed symbols are saturated data.

CONCLUSIONS

The pulse-echo method of measuring ultrasonic wave attenuation is shown to be a good method for determining shear and compressional energy dissipation in saturated basalts. By determining shear wave attenuation, known relationships between compressional wave attenuation and physical properties are extended to shear propagation. Additionally, calculating shear and compressional wave quality factors allows for a qualitative investigation of mechanisms responsible for loss with both wave types and a quantitative investigation of the effect of saturation on anelasticity.

Shear and compressional waves are less attenuated at elevated pressures due to the closure of microcracks. Compressional and shear wave data decrease with increasing pressure. The linear shear wave pressure dependence is probably due to the relatively low pressures for which shear attenuation was measured. Calculated Q_p and Q_s both increase with increasing pressure.

Attenuation and Q are also dependent on porosity and density. Both shear and compressional wave data record a negative linear gradient with increasing porosity and decreasing density. Shear and compressional wave attenuation are highly dependent on the degree of saturation. Experiments conducted for both dry and water-saturated basalt indicate that shear attenuation increases by as much as 51 per cent for a fluid-saturated sample, while compressional wave attenuation increases by 62 per cent in the same basalt.

By combining Q_s, Q_p, V_p and V_s, dry versus saturated rock conditions are delineated. Q_s/Q_p values are minimized under saturated conditions and maximized under dry conditions, although experiments were not performed under partial water saturation. V_p/V_s values are minimized under dry conditions and increase for saturated rock. Therefore, results that show low Q_s/Q_p (<0.40) and high V_p/V_s (>1.75) indicate a saturated rock state. Values beyond these thresholds indicate dry conditions. Q_s/Q_p values also support evidence for a 'squirt' flow attenuation mechanism in saturated basalt.

Laboratory attenuation results compare well with field measurements, but reasons for this agreement are not fully understood. At seismic frequencies, heterogeneities and scattering are possible loss mechanisms; however, if heterogeneities occur on a scale smaller than the seismic wavelength, scattering will not dominate attenuation. In addition, intrinsic attenuation at seismic frequencies is not zero; therefore, some frictional or viscous flow attenuation mechanism is present. We suggest that a mechanical loss mechanism at both high and low frequencies is time-dependent fluid flow, but strong evidence does not exist to indubitably determine its relative importance.

ACKNOWLEDGMENTS

We would like to thank R. L. Carlson and A. Beck for their constructive reviews of the manuscript. Funding for this project was provided by the Office of Naval Research and the National Science Foundation Continental Dynamics Program.

REFERENCES

Benson, G.C. & Kiyohara, O., 1976. Table of integral functions describing diffraction effects in the ultrasonic field of a circular piston source, *Depository of Unpublished Data,* National Science Library, National Research Council of Canada, Ottawa, Canada.

Biot, M.A., 1956. Theory of propagation of elastic waves in a fluid-saturated porous solid, II. High-frequency range, *J. acoust. Soc. Am.*, **28,** 179–191.

Birch, F., 1960. Velocity of compressional waves in rocks to 10 kilobars, *J. geophys. Res.*, **65,** 1083–1093.

Brennan, B.J. & Stacey, F.D., 1977. Frequency dependence of elasticity of rock-test of seismic velocity dispersion, *Nature,* **268,** 220–222.

Carlson, R.L. & Herrick, C.N., 1990. Densities and porosities in the oceanic crust and their variations with depth and age, *J. geophys. Res.*, **95,** 9153–9170.

Christensen, N.I., 1972. Compressional and shear wave velocities at pressures to 10 kilobars for basalts from the East Pacific Rise, *Geophys. J. R. astr. Soc.*, **28,** 425–429.

Christensen, N.I., 1985. Measurements of dynamic properties of rock at elevated pressures and temperatures, in *Measurement of Rock Properties at Elevated Pressures and Temperatures,* pp. 93–107, eds Pincus, H.J. & Hoskins, E.R., American Society for Testing and Materials, Philidelphia, PA.

Christensen, N.I., 1996. Poisson's ratio and crustal seismology, *J. geophys. Res.*, **101,** 3139–3156.

Christeson, G.L., Wilcock, W.S.D. & Purdy, G.M., 1994. The shallow attenuation structure of the fast-spreading East Pacific Rise near 9°30'N, *Geophys. Res. Lett.*, **21,** 321–324.

Dvorkin, J. & Nur, A., 1993. Dynamic poroelasticity: a unified model with the squirt and Biot mechanisms, *Geophysics,* **58,** 524–533.

Gardner, G.H.F., Wyllie, M.R.J. & Dorschak, D.M., 1964. Effects of pressure and fluid saturation on the attenuation of elastic waves in sands, *J. Petrol. Techn.*, **16,** 189–198.

Goldberg, D. & Sun, Y.F., 1997. Attenuation differences in layer 2A in intermediate- and slow-spreading oceanic crust, *Earth planet. Sci. Lett,* **150,** 221–231.

Goldberg, D. & Yin, C.-S., 1994. Attenuation of p-waves in oceanic crust: multiple scattering from observed heterogeneities, *Geophys. Res. Lett.*, **21,** 2311–2314.

Gordon, R.B. & Davis, L.A., 1968. Velocity and attenuation of seismic waves in imperfectly elastic rock, *J. geophys. Res.*, **73,** 3917–3935.

Green, D.H., 1989. Poroelasticity of sedimentary rocks, *PhD Thesis,* University of Wisconsin-Madison, Madison, WI.

Green, D.H., Wang, H.F. & Bonner, B.P., 1993. Shear wave attenuation in dry and saturated sandstone at seismic to ultrasonic frequencies, *Int. J. Rock Mech. Min. Sci. Geomech. Abs.*, **30,** 755–761.

Holbrook, W.S., Gajewski, P., Krammer, A. & Prodehl, C., 1988. An interpretation of wide-angle compressional and shear wave data in southwest Germany: Poisson's ratio and petrological implications, *J. geophys. Res.*, **93,** 12 081–12 106.

Hyndman, R.D., Christensen, N.I. & Drury, M.J., 1979. Seismic velocities, densities, electrical resistivities, porosities, and thermal conductivities of core samples from boreholes into the islands of Bermuda and The Azores, in *Deep Drilling Results in the Atlantic Ocean: Ocean Crust,* pp. 94–112, eds Talwani, M., Harrison, C.G. & Hayes, D.E., AGU, Washington, DC.

Jacobson, R.S. & Lewis, B.T.R., 1990. The first direct measurements of upper oceanic crustal compressional wave attenuation, *J. geophys. Res.*, **95,** 17 417–17 429.

Johnston, D.H. & Toksoz, M.N., 1980. Ultrasonic, p, and s wave attenuation in dry and saturated rocks under pressure, *J. geophys. Res.*, **85,** 925–936.

Johnston, J.E. & Christensen, N.I., 1997. Seismic properties of layer 2 basalts, *Geophys. J. Int.*, **128,** 285–300.

Khimunin, A.S., 1972. Numerical calculations of the diffraction corrections for the precise measurement of ultrasound absorption, *Acoustica,* **27,** 173–181.

Kowallis, B.J., Roeloffs, E.A. & Wang, H.F., 1982. Microcrack studies of basalts from the Iceland Research Drilling Project, *J. geophys. Res.*, **87** (B8), 6650–6656.

Lewis, B.T.R. & Jung, H., 1989. Attenuation of refracted seismic waves in young oceanic crust, *Bull. seism. Soc. Am.*, **79,** 1070–1088.

Mavko, G.M. & Nur, A., 1979. Wave attenuation in partially saturated rocks, *Geophysics,* **44,** 161–178.

Murphy, W.F., 1982. Effects of partial water saturation on attenuation in Massilon sandstone and Vycor porous glass, *J. acoust. Soc. Am.*, **71,** 1458–1468.

Papadakis, E.P., Fowler, K.A. & Lynnworth, L.C., 1973. Ultrasonic attenuation by spectrum analysis of pulses in buffer rods: method and diffraction corrections, *J. acoust. Soc. Am.*, **53,** 1336–1343.

Rutledge, J.T. & Winkler, H., 1987. Attenuation measurements in basalt using vertical seismic profile data from the eastern Norwegian Sea, *SEG Expanded Abstracts,* 711–713.

Shapiro, S.A. & Muller, T.M., 1999. Seismic signatures of permeability in heterogeneous porous media, *Geophysics,* **64,** 99–103.

Swift, S.A., Lizarralde, D., Stephen, R.A. & Hoskins, H., 1998. Seismic attenuation in the upper oceanic crust at Hole 504B, *J. geophys. Res.*, **103,** 27 193–27 206.

Tittmann, B.R.H., Nadler, L., Ahlberg & Cohen, E.R., 1977. Q measurements under confining pressure, in *High Pressure Science and Technology,* Vol. 2, pp. 255–262, eds Timmerhaus, K.D. & Barber, M.S., Plenum, New York.

Toksoz, M.N., Johnston, D.H. & Timur, A., 1979. Attenuation of seismic waves in dry and saturated rocks: I, laboratory measurements. *Geophysics*, **44**, 681–690.

Tompkins, M.J. & Christensen, N.I., 1999. Effects of pore pressure on compressional wave attenuation in a young oceanic basalt, *Geophys. Res. Lett.*, **26**, 1321–1324.

Volarovitch, M.P. & Gurvitch, A.S., 1957. Investigation of dynamic moduli of elasticity for rocks in relation to temperature, *Bull. Acad. Sci. USSR, Geophys. Ser.*, **4**, 1–9.

Walsh, J.B., 1966. Seismic wave attenuation in rock due to friction, *J. geophys. Res.*, **71**, 2591–2599.

Weiner, A.T., Manghnani, M.H. & Raj, R., 1987. Internal friction in tholeiitic basalts, *J. geophys. Res.*, **92**, 11 635–11 643.

Wepfer, W.W., 1989. Application of laboratory velocities and attenuation data to the Earth's crust, *PhD Thesis,* Purdue University, West Lafayette, IN.

Wepfer, W.W. & Christensen, N.I., 1990. Compressional wave attenuation in oceanic basalts, *J. geophys. Res.*, **95**, 17 431–17 439.

Wepfer, W.W. & Christensen, N.I., 1991a. Q structure of the oceanic crust, *Mar. Geophys. Res.*, **13**, 227–237.

Wepfer, W.W. & Christensen, N.I., 1991b. A seismic velocity-confining pressure relation, with applications, *Int. J. Rock Mech. Mining Sci., Geomechanics Abstracts*, **28**, 451–456.

White, D.J. & Clowes, R.M., 1994. Seismic attenuation structure beneath the Juan de Fuca ridge from tomographic inversion of amplitudes, *J. geophys. Res.*, **99**, 3043–3056.

Wilcock, W.S.D., Soloman, S.C., Purdy, G.M. & Toomey, D.R., 1992. The seismic attenuation structure of a fast-spreading mid-ocean ridge, *Science*, **258**, 1470–1474.

Wilcock, W.S.D., Soloman, S.C., Purdy, G.M. & Toomey, D.R., 1995. Seismic attenuation structure of the East Pacific Rise near 9°30′N, *J. geophys. Res.*, **100**, 24 147–24 165.

Winkler, K.W. & Nur, A., 1982. Seismic attenuation: effects of pore fluids and frictional sliding, *Geophysics*, **47**, 1–15.

Winkler, K.W. & Plona, T.J., 1982. Technique for measuring ultrasonic velocity and attenuation spectra in rocks under pressure, *J. geophys. Res.*, **87**, 10 776–10 780.